RSC Advances

PAPER

View Article Online
View Journal | View Issue

Cite this: *RSC Adv.*, 2024, **14**, 15627

Electrocatalytic water treatment of per- and polyfluoroalkyl substances reduces adsorbable organofluorine and bioaccumulation potential†

Zunhui Lin,[a] Mahmut S. Ersan,[b] Sergi Garcia-Segura,[a] François Perreault[c] and Paul Westerhoff *[a]

Per- and polyfluoroalkyl substances (PFAS) are pervasive in industrial processes, eliciting public concern upon their release into municipal sewers or the environment. Removing PFAS from the environment has become an urgent need. However, because potential endpoints span from energy-intensive complete mineralization to partial PFAS transformation, understanding and developing metrics for evaluating PFAS treatment can be a challenge. The goal of this study was to evaluate and compare the effectiveness of electrocatalytic degradation of PFAS with boron-doped diamond (BDD) electrodes using four techniques: LC-MS/MS target analysis, fluoride ion (F^-), adsorbable organofluorine (AOF), and bioaccumulation potential using lipid-bilayer partition (LBP) tests. After 3 hours of electrocatalysis, >99% perfluorooctanoic acid (PFOA) degradation was achieved and corresponded with 84% conversion to F^-, which was substantial – though intentionally not complete – defluorination. For the same 3 hour treatment time, AOF and LBP coefficient were reduced by 95% and 83%, respectively. LBP's detection limit was 2 orders of magnitude higher than that of AOF, so the positive correlation observed between LBP and AOF ($r = 0.86$) suggests AOF's practical utility as a design metric for assessing bioaccumulation potential of various organofluorine transformation by-products.

Received 31st March 2024
Accepted 2nd May 2024

DOI: 10.1039/d4ra02448f

rsc.li/rsc-advances

1. Introduction

Per- and polyfluoroalkyl substances (PFAS) are a large group of synthetic chemicals with over 5000 compounds that have been in commercial use since the 1940s.[1] Sources of PFAS include fluorochemical plants,[2,3] electronics production facilities,[4,5] airports and firefighting sites.[6] Owing to their hydrophobic and oleophilic properties, PFAS readily adsorb, partition, and accumulate in diverse environmental compartments, including sediments,[7,8] soils,[9] biosolids,[10] and biological tissues.[11,12] Removing and treating PFAS in industrial wastewaters, contaminated groundwaters and other water sources is important to prevent adverse human and ecological impacts.

The potential hazards from PFAS include human carcinogenicity,[13] reproductive issues,[14] and immunotoxicity.[15] In 2023 and 2024, the United States Environmental Protection Agency (USEPA) proposed and then finalized drinking water maximum contaminant levels (MCLs) for six individual PFAS.[16] This included MCLs of 4 ng L^{-1} for perfluorooctanoic acid (PFOA) and perfluorooctanesulfonic acid (PFOS), plus a hazard index (HI) value based upon a concentration normalized sum of shorter chain PFAS including hexafluoropropylene oxide dimer acid and its ammonium salt (GenX), perfluorobutanesulfonic acid (PFBS), perfluorononanoic acid (PFNA), and perfluorohexane sulfonate (PFHxS). The Hazard Index is a long-established approach that EPA regularly uses to understand health risk from a chemical mixture (*i.e.*, exposure to multiple chemicals). Therefore, it is imperative that any transformation-based treatment technology account for not only the parent PFAS but also by-products formed during treatment.

The USEPA Hazard Index HI is made up of a sum of fractions. Each fraction compares the level of each PFAS measured in the water to the health-based water concentration. In April 2024 the USEPA established final MCLs of 4 ng L^{-1} for PFOA and PFOS, plus 10 ng L^{-1} for hexafluoropropylene oxide dimer acid and its ammonium salt (GenX), perfluorononanoic acid (PFNA) and perfluorohexane sulfonate (PFHxS). When more than one of the later 3 PFAS occur at above 10 ng L^{-1}, then a calculated HI must be below 1.0.[16]

These seminal drinking water regulations are expected to have a cascading impact on PFAS limits for industrial discharge into sewers and discharge at municipal wastewater treatment plants (WWTPs). An increasing number of states already regulate PFAS

[a]*Nanosystems Engineering Research Center for Nanotechnology-Enabled Water Treatment, School of Sustainable Engineering and the Built Environment, Arizona State University, Tempe, Arizona, USA. E-mail: p.westerhoff@asu.edu; Tel: +480-965-2885*

[b]*Department of Civil Engineering, University of North Dakota, Grand Forks, ND, USA*

[c]*Department of Chemistry, University of Quebec in Montreal, Succ. Centre-Ville, CP 8888, Montreal, QC, H3C 3P8, Canada*

† Electronic supplementary information (ESI) available. See DOI: https://doi.org/10.1039/d4ra02448f

in WWTP biosolids;[17] for example, Wisconsin limits land disposal of biosolids containing more than 150 μg kg^{-1} PFAS.[18] With pending regulation of PFAS in municipal wastewater biosolid disposal or drinking water, there is a need for industries discharging wastewater containing PFAS to municipal sewers or the environment to implement on-site PFAS treatment systems. Regulations may dictate mandatory treatment, often enforced by analyzing for targeted PFAS using liquid chromatography tandem mass spectrometry (LC-MS/MS). However, a holistic sustainability perspective, or even a legacy chemical legal concern, may necessitate PFAS treatment design performance metrics that go beyond targeted analytical measurements.

Advanced analytical methods can quantify some target organofluorine compounds at part-per-trillion (ppt) levels. Standard methods (*e.g.*, EPA 537.1, 533, and 1633) have been used to measure the occurrence of PFAS in water and solid matrices, but the methods are limited to only detect 17 to 40 target PFAS.[19] Non-target LC-MS/MS analysis would be required to measure all partially-defluorinated PFAS treatment intermediates, and closing the fluorine mass balance has been challenging and costly. Although non-target analysis is a powerful research tool for PFAS,[3] it is unlikely to be useful in regulatory frameworks. While the ultimate goal of any PFAS treatment technology could strive to achieve complete mineralization, producing only fluoride ion (F^-) and other inorganic by-products (*e.g.*, carbon dioxide, sulfate). Quantifying sub microgram per liter of F^- in water is not currently possible, and detection at even sub milligram per liter conversion of PFAS to F^- can be especially in complex industrial wastewaters where F^- can occur at over 100 mg L^{-1}.[20] Alternative approaches such as adsorbable organofluorine (AOF) have been proposed by the European Union (EU), and measure total organic fluorine (TF) through combustion of PFAS adsorbed on activated carbon (AC) to quantify unknown PFAS.[21]

Bioaccumulation of PFAS is an important hazard endpoint. A variety of bio-analytical methods using aquatic organisms[22] or human tissues[23] have been used to derive indices such as bioconcentration factors (BCF) or biomagnification factors. However, these methods vary greatly depending on the body part of a selected biota and require complex sampling across multiple trophic levels.[24,25] For example, PFOA has a whole body BCF of 1.85 ± 0.08 L kg^{-1} in zebrafish (*Danio rerio*)[26] and a BCF of $10^{2\pm0.02}$ L kg^{-1} in zebrafish larvae.[27] PFOA also showed steady state BCF of 3.9–10 kg L^{-1} for fathead minnows (*Pimephales promelas*) and 0.2–5.1 kg L^{-1} for mussels.[28] To assess the bioaccumulation potential of PFAS with varying chain lengths, an *in vitro* assay utilizing lipid-bilayers known as Transil^{XL} has proven effective in distinguishing binding affinities for a spectrum of PFAS.[29] Lipid bilayers measurements have largely been limited to individual and target PFAS, rather than on mixtures containing unknown components commonly found in wastewaters. A knowledge gap exists concerning the bioaccumulation potential of by-products resulting from PFAS degradation using emerging engineered treatment processes.

To mitigate the environmental exposure and hazard of PFAS, emerging technologies including plasma,[30] electrochemical treatment,[31,32] photocatalysis,[33] and other advanced reduction or oxidation processes[34] all show promise to defluorinate PFAS in wastestreams.[35] Selecting appropriate metrics to determine the size and input energy of PFAS treatment systems remains elusive, and they could encompass a spectrum from energy-intensive complete defluorination and mineralization to partial PFAS transformation.

Destructive treatment technologies hold tremendous potential to hazard of PFAS by converting longer chain PFAS into shorter chain byproducts. Heterogeneous catalysis in general and electrocatalysis more specifically show promise for treating industrial wastewaters because hydrophobic PFAS tend to partition to surfaces where they are concentrated and can be readily degraded at the interface rather than competing with other solutes in the bulk solution at higher concentrations.[35,36] Shorter chain PFAS compounds, in part owing to their lower hydrophobicity compared against longer chain PFAS, often have lower bioaccumulation potential.[37] Thus, hydrophobicity affects both treatment efficiency and organism-based hazard. Currently, there is a lack of understanding how catalytic treatment of PFAS impacts bioaccumulation potentials and what endpoints could represent bioaccumulation.

To fill this knowledge gap, our study evaluated and compared techniques to track treatment effectiveness during one representative catalytic PFAS treatment system, namely electrocatalysis using BDD electrode, which we previously showed to be effective in removing PFAS from real and model wastewaters.[31] Four techniques were used to assess effectiveness: targeted PFAS measurement by LC-MS/MS, F^- measurement by ion chromatography (IC), adsorption capacity on activated carbon (*i.e.*, AOF analysis), and bioaccumulation potential using lipid bilayer partitioning assays (Transil^{XL}). Comparing the four analytical techniques may facilitate the selection and justification of proper design metric endpoints for treating PFAS in wastewater.

2. Materials and methods

2.1 Model water containing PFOA

Based on our prior work with model and real industrial wastewater electrocatalysis studies,[31] we selected a stock solution with high PFOA and low background organics to enable using all PFAS analytical tools of interest. This approach allowed us to work about the detection limits of the combustion ion chromatography (CIC) and within the working concentration range of the Transil^{XL} analytical workflow. PFOA (95% purity, cat. No. 171468, Sigma Aldrich), PFBA (98%, cat. no. 164194) and PFHxA (>97%, cat. no. 29226) were also purchased from Sigma Aldrich (Table S1†). Accordingly, our working solution was prepared using 40 μM PFOA with a 15 mM electrolyte of Na_2SO_4 (>99%, anhydrous, Sigma Aldrich) in ultrapure (Millipore, 18.2 MΩ cm) water (UPW), with no further addition of any pH buffer, salts, acids or bases. The initial pH of this model water was 5.6. Internal standards (IS) were prepared using a ^{13}C isotope-labeled methanol-based 24 MPFAS-MXA mixture obtained from Wellington Laboratories (Guelph, ON).

2.2 Electrocatalytic reactor

As demonstrated in our prior work, an electrochemical reactor with BDD cathodes and anodes, as illustrated in Fig. S1,† has

optimal performance for PFAS degradation in model and real industrial wastewaters.[31] Details of BDD electrodes are provided in Text S1.† Briefly, electrocatalysis experiments were performed in a 150 mL Pyrex glass beaker using 120 mL of PFOA solution. The electrode backs were covered by vinyl tape (Scotch, Saint Paul, MN) to achieve a geometric effective surface area of 5 cm^2. Electrodes were submerged in the testing solution, and the interelectrode distance was kept at 1 cm. A constant 60 mA cm^{-2} current density was maintained by a power supply (TENMA model 72–8340A, England) with a cell potential of 40–45 V. The solution was stirred continuously at 700 rpm to ensure complete mixing and sufficient mass transport between the electrode surfaces and the bulk liquid.

2.3 Sample collection over time

Sample aliquots of 2 mL were withdrawn for analysis at 0, 10, 30, 60, 120, and 180 minutes after electrocatalysis initiation. The cumulative aliquot volume during the experiment accounted for less than 20% of the initial volume. Each 2 mL aliquot was prepared as follows prior to analysis: 10 μL was subjected to a 100-fold dilution for LC-MS/MS target analysis, 1 mL was diluted tenfold for IC measurement of F^-, 20 μL was directly injected into the CIC to track the TF in the system, 200 μL was mixed with 50 mL of deionized water and acidified to pH < 2 using 1 N H_2SO_4 for AOF, and 160 μL was utilized for the Transil^{XL} assay.

2.4 PFASs target analysis

Because we used PFOA as the initial PFAS, we only measured carboxylated (PFCA) target compounds (PFOA, PFHxA, PFBA) as transformation by-products. These were measured using a LC-MS/MS (Agilent 1290 & 6490) operating in electrospray negative ionization (ESI) mode.[38] Method details, quality assurance, and quality control are described in Text S2 and S3.† Details on instrumental parameters and mobile phase gradient are given in Table S2 through S5.† Limits of detection (LoD) and quantification (LoQ) were defined by the concentrations with 3 times signal to noise (S/N) and 10 times S/N, respectively. The LoD of PFOA for this study was 3 ng L^{-1}. The LoQ of PFOA was 10 ng L^{-1}. Details of LoDs and LoQs for all other target PFAS are given in Table S6.†

2.5 Inorganic fluoride ion (F^-) measurement

F^- concentrations were measured by IC (Metrohm 930 Compact IC Flex analyzer and 858 Professional Sample Processor (Herisau, Switzerland)). The instrument was equipped with an A Supp 5 analytical column (4 mm × 150 mm) in conjunction with an A Supp 5 guard column. An injection loop of 20 μL achieved a 1 μM F^- minimum detection limit. Eluent composed of 1 mmol L^{-1} Na_2CO_3 and 3.2 mmol L^{-1} $NaHCO_3$ flowed at 0.7 mL min^{-1} through the column.

2.6 AOF quantification

AOF was measured by passing 50 mL aliquots, diluted from 200 μL of the collected electrochemical time-dependent sample, at 3 mL min^{-1} onto two packed 40 mg activated carbon (AC) cartridges (Analytik Jena, Germany) in series on an APUsim autosampler. The low fluorine activated carbon has a BET surface area of ~500 m^2 g^{-1}, and a total mass of 80 mg was used. AC cartridges were washed with 20 mL of 0.1% NH_4OH to remove inorganic F^-.[21,39] The PFAS-loaded AC samples were combusted for 20 minutes at 1050 °C under 300 mL min^{-1} O_2 by the CIC (details were described in previous studies[20,40] and operating parameters for this study are listed in Table S7†). Table S8† shows that AOF recovery rates increase with carbon chain length.[41] Comparable with previous studies,[41] recovery rates of PFBA (57 ± 20%), PFHxA (69 ± 11%), and PFOA (110 ± 2.9%) improved with chain length.

The theoretical TF of this electrocatalysis system based on the initial 40 μmol L^{-1} $C_8HF_{15}O_2$ was 600 μM as fluorine. The TF measured by CIC during the 3 hours electrocatalysis was within ±30% of the theoretical TF as shown in Fig. S3.† A 20% difference in CIC response between organofluorine and F^- was common,[42] so we assumed that TF was conservative at its theoretical value.

Unidentified organofluorine (UIOF) and non-adsorbable organofluorine (NAOF) were defined as the concentration in μM of total organofluorine not quantified by target analysis and AOF, respectively, and calculated as follows in the following equations:

$$\mathrm{TF} = n_{\mathrm{PFOA}} C_{0,\mathrm{PFOA}} \quad (1)$$

$$\mathrm{UIOF} = \mathrm{TF} - \sum_{\mathrm{i}} n_{\mathrm{i}} C_{\mathrm{i}} - [\mathrm{F}^-] \quad (2)$$

$$\mathrm{NAOF} = \mathrm{TF} - \mathrm{AOF} - [\mathrm{F}^-] \quad (3)$$

where TF is 600 μM in this study ($n_{\mathrm{PFOA}} = 15$ fluorine; $C_{0,\mathrm{PFOA}} =$ 40 μM); C_{i} is the target PFAS concentration (μM), n_{i} is the number of fluorine atoms in that PFAS molecule, $[F^-]$ is fluoride ion concentration (μM), and AOF (μM) was the measured concentration based on the CIC method.

2.7 Bioaccumulation potential using Transil^{XL} suspend lipid bilayer assay

Transil^{XL} Intestinal Absorption kits were obtained from Sovicell GmbH (Leipzig, Germany) for use as a modeled bioaccumulation assay.[29] This assay utilizes 12 × 8 wells microtiter plates, with each sample utilizing one column of 8 wells as shown in Fig. S2.† Within each column, there are 2 reference wells and 6 wells containing 0.048, 0.086, 0.156, 0.281, 0.505, and 0.907 μL of immobilized biological phase in 240 μL phosphate buffer saline (PBS) solution, which helps maintain pH and osmotic pressure. The Transil^{XL} beads used in the assay are phosphatidylcholine liposomes vesicles with a diameter of 15 μm. The Transil^{XL} assay was preserved, incubated, mixed and separated following an established protocol with details in Text S3.[43]

A partition-based model was developed to quantify the affinity of organofluorine to lipid bilayer tissues using eqn (4):

$$\mathrm{LBP} = C_{\mathrm{S}}/C_{\mathrm{L}} \quad (4)$$

where C_S (μmol PFAS/kg lipid) and C_L (μmol PFAS/L) are the PFAS concentration associated with lipid or aqueous phase, respectively.

For single PFCA compound, the LBP value was derived following the calculation in Text S4.† The final LBP value is shown in eqn (5):

$$\mathrm{LBP} = \frac{C_0 V_1 - C_L V_{aq}}{C_L V_s \rho_s} \quad (5)$$

where C_0 (μmol L^{-1}) is the standard stock concentration spiked into the Transil^{XL} assay, V_1 is volume of sample (20 μL), V_{aq} is the total liquid volume inside a Transil^{XL} vial after sample addition (260 μL), V_s (μL) is the volume of Transil^{XL} lipid beads, and ρ_s is the lipid bilayer density (1.05 kg L^{-1}).

CIC analytical approaches were also used for quantifying fluoride levels in multi-solute samples. Solid phase lipids inserted on CIC ceramic boats instead of PFAS-loaded AC. Liquid phase aliquots (100 μL of supernatant) from the LBP assay were collected, placed in the CIC boat and used to quantify and then calculate TF_{sup} (μmol). A 100 μL aliquot of well-mixed liquid and solids from the remaining contents in Transil^{XL} vial was collected, placed in the ceramic boat, and analyzed using CIC to measure TF adsorbed onto LBP solid (TF_{sed} (μmol)). The final LBP was calculated by eqn (6) with details explained in Text S5:†

$$\mathrm{LBP} = \frac{1.4(\mathrm{TF_{sed}} - \mathrm{TF_{sup}})V_{tot}}{2.6\mathrm{TF_{sup}} V_s \rho_s} \quad (6)$$

where V_{tot} is the total volume of liquid (260 μL) in a Transil^{XL} vial. The minimum working concentration of Transil^{XL} assay was calculated based on CIC detectable TF_{sup} in vial G to be 23 μM PFOA (Text S6†). This study started with 40 μM, which guaranteed that TF in all Transil^{XL} kits would be quantifiable by CIC. A control experiment applied 600 μM F^- as NaF to test the LBP of F^-.

3. Results and discussion

3.1 Electrochemical transformation of PFOA

Utilizing the BDD anode and cathode for electrocatalysis resulted in a gradual degradation of PFOA over time. The primary electrochemical PFOA transformation was likely initiated by direct electron transfer from PFOA to active sites on the BDD surface,[44,45] followed by decarboxylation to form $C_7H_{15}^{\cdot}$ and chain shortening cycles to lose $-CF_2-$ units.[32,46] Fig. 1 shows that approximately 50% of the initial PFOA degraded within the first hour and reached 94% after two hours. After three hours of electrocatalytic treatment, PFOA was below the detection limit, signifying >99% removal. The observed change in PFOA to below the detection limit was desirable because it allowed for subsequent analysis of AOF and LBP for varying degree (0 to >99%) of PFOA transformation.

Despite near complete PFOA removal, complete defluorination of PFOA was not achieved after 3 hours of treatment. From the defluorination curve in Fig. 1, F^- increased steadily, reaching 505 μM after 3 hours, overall, the F^- yield from PFOA was only 84% at the point where >99% of the initial PFOA was

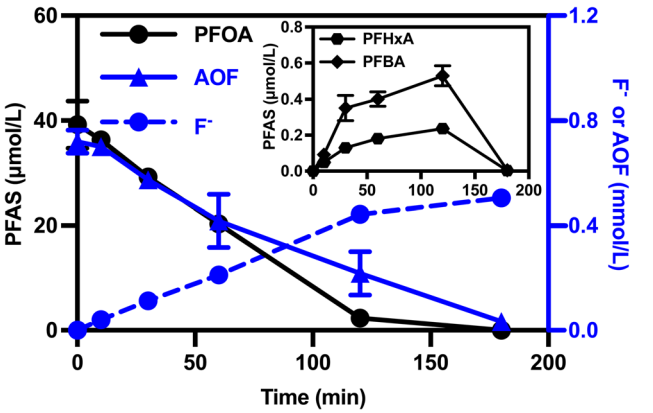

Fig. 1 Evolution of target analytes, AOF, and F^- during 40 μM PFOA (TF = 600 μM fluorine) electrocatalysis at 60 mA cm^{-2} current density over 3 hours. AOF and F^- correspond to the right-hand secondary y-axis. By-products PFHxA and PFBA are shown in the insert. Error bars depict standard deviations of duplicated experiments.

degraded. This likely occurred because PFCA intermediates were less hydrophobic, exhibited reduced affinity towards the BDD active surface, and consequently were more difficult to defluorinate.[31]

Measuring AOF enables assessment of changes in target plus non-target organofluorine and can distinguish degradation from defluorination throughout the electrocatalysis process.[47] Fig. 1 shows AOF reduction paralleled PFOA loss in the first hour and declined more slowly than PFOA after the first hour. After 3 hours of electrochemical treatment, there was 34 μM AOF, which was 6% of the 600 μM fluorine initially added as PFOA. The faster decrease of AOF compared with the increase of F^- suggested that intermediate organofluorine products were not fully mineralized and did not release F^-. Longer chain organofluorine transformed into shorter chain PFAS with reduced AOF recovery,[48] but it was still partially retained on activated carbon.

Evolution of shorter chain target by-products was observed. As illustrated in Fig. 1, short chain by-products PFHxA and PFBA accumulated during the first 2 hours and reached a maximum of 0.24 μM and 0.54 μM, respectively, which were much lower concentrations than the initial 40 μM PFOA. These by-products originated from the breakdown of PFOA and were subject to electrocatalysis simultaneously. The PFBA was more challenging to degrade due to its lower affinity with the electrode surface,[31,49] so PFBA accumulated at higher concentration than PFHxA. The pattern of formation and subsequent degradation of PFHxA and PFBA aligned with findings from previous studies.[31,49] However, even at their maximum concentrations, target by-products cumulatively accounted for less than 2% of the fluorine initially added in the reactor.

The USEPA Hazard Index (HI) is made up of a sum of fractions. Each fraction compares the level of each PFAS measured in the water to the health-based water concentration. In April 2024 the USEPA established final MCLs of 4 ng L^{-1} for PFOA and PFOS, plus 10 ng L^{-1} for hexafluoropropylene oxide dimer acid and its ammonium salt (GenX), perfluorononanoic acid

(PFNA) and perfluorohexane sulfonate (PFHxS). When mixture of two or more specific compounds (PFNA, PFHxS, HFPO-DA, and PFBS) are present, the HI must below a value of unity. Each fraction compares the level of each PFAS measured in the water to the highest level determined not to have risk of health effects. Herein we calculated the HI based upon eqn (7) using measured concentrations after each timepoint from our electrocatalysis treatment system:

$$\mathrm{HI} = \frac{[\mathrm{GenX}]}{10\ \mathrm{ng/L}} + \frac{[\mathrm{PFBS}]}{2000\ \mathrm{ng/L}} + \frac{[\mathrm{PFNA}]}{10\ \mathrm{ng/L}} + \frac{[\mathrm{PFHxS}]}{9.0\ \mathrm{ng/L}} \quad (7)$$

Concentrations of each were at low levels after 3 hours electrocatalysis, but their cumulative effect could pose significant health risks. The Hazard Index is an established USEPA approach used to understand health risk from chemical mixtures.[50] A hazard index value at or below 1 suggests that cumulative exposure is generally considered safe and unlikely to cause significant adverse health effects, while a hazard index value above 1 indicates potential health risks, necessitating further assessment and possibly mitigation measures to lower such exposures. However, a hazard index of 0 does not imply that there are no concerns associated with PFAS. Since no carboxylated PFAS are part of the current HI calculation, the HI value throughout our experiments using solely PFOA as the initial model PFAS was 0. Future work using other PFAS should always consider reporting HI values.

3.2 Fluorine mass balance during electrocatalytic treatment

Fig. 2A presents the distribution of fluorine species over time based on target PFAS, F^-, and UIOF. PFOA accounted for <50% of the fluorine after 1 hour of treatment and <6% of the fluorine after 3 hours. Concurrently, the portion of F^- increased from 0% to 74% after 2 hours, and further rose to 84% after 3 hours. The maximum contribution from target by-products (PFHxA and PFBA shown in Fig. S4†) was <1% of total fluorine. The peak 19% of UIOF occurred after 2 hours of treatment. The observation that UIOF remains below 20% of the total fluorine in the system indicates that target analysis together with F^- accounts for most of the mass balance. UIOF likely includes polar short chain compounds such as trifluoroacetic acid (TFA), but quantifying that would require modification of LC-MS/MS methods.[51]

Fig. 2B shows how surrogate index of AOF closed the fluorine mass balance during treatment. From 0 to 2 hours, AOF's contribution decreased from 100% to 30%, and it further decreased to 5% at 3 hours. NAOF was not detected until 0.5 hour of treatment, reaching a maximum of 11% at 3 hours. Similar to UIOF, NAOF portions may experience losses during AOF extraction or through evaporation of volatiles escaping from the electrochemical reactor.[52] The NAOF was also likely to include TFA or other polar PFAS that are poorly retained on the AOF sorbent. Combining AOF with F^- accounted for >80% of the total fluorine in this electrocatalysis system, indicating AOF was a good approximation of the summation of target compounds and non-target by-products.

3.3 Validation of LBP using PFOA

We explored lipid partitioning as a potential PFAS treatment design metric. LBP is a partition based descriptor introduced to study chemical interactions with cell membranes.[53] LBP has not yet been applied to assess PFAS electrochemical transformation by-products. Before applying the LBP assay on the unknown organofluorine mixture, LBP of target PFAS was first measured by LC-MS/MS and compared with recorded literature values. PFOA stock solutions of 4.8, 40, and 1000 μM were spiked into the Transil^{XL} assay and resulted in an isotherm shown in black in Fig. 3. There was no statistical difference ($p = 0.68$) on LBP among the three concentration intervals. The resulting LBP of $10^{3.0\pm0.2}$ L kg^{-1}, which was less than 0.5 log lower compared with the reported value of $10^{3.51\pm0.07}$,[29] was considered acceptable for partitioning models.[29] Transil^{XL} partition isotherms for PFBA and PFHxA were measured by adding 20 μL of 23.4 μM PFBA and 3.2 μM of PFHxA and they also resulted in LBP values within 0.5 log of literature values, $10^{1.7\pm1.9}$ L kg^{-1} for PFBA and $10^{2.5\pm2.3}$ L kg^{-1} for PFHxA (results shown in Fig. S6† and summarized in Table S9†). Thus, the accuracy and reproducibility of the assay was considered validated using liquid-phase

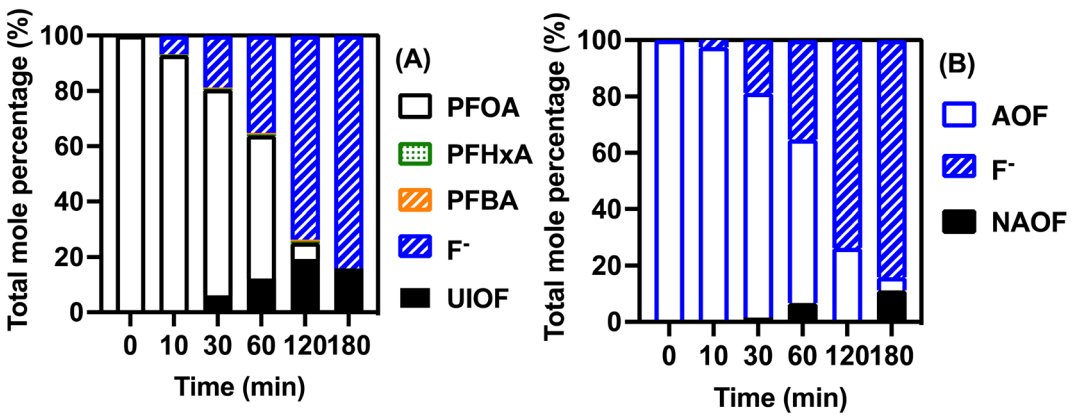

Fig. 2 Stacked bar chart illustrating mass balances for samples collected during electrocatalysis on an initial 40 μM PFOA solution. (A) Target PFAS, F^-, and UIOF. (B) AOF, F^-, and NAOF. Additional changes based upon measured PFHxA and PFBA concentrations are presented in Fig. S4.†

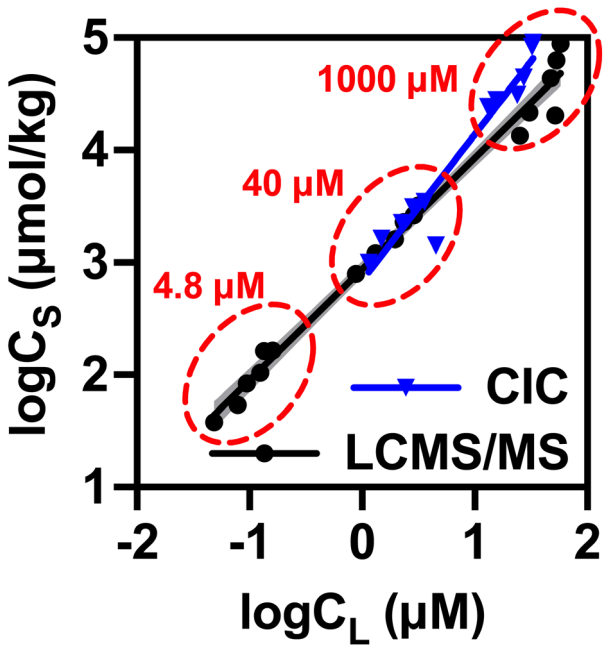

Fig. 3 PFOA partition isotherms between aqueous phase by LC-MS/MS or Transil^{XL} phosphatidylcholine liposomes bead solid phase analysis by CIC. Solid line shows regression model fit of the two datasets. Shaded areas indicate the 95% CI of linear regression. The spike concentrations of PFOA for each part of the isotherm are noted in red.

PFAS. In order to apply it to electrochemical by-products we further compared liquid-with solid-phase partition coefficients.

To compliment target PFAS remaining in solution after exposure to the lipid bilayer, we cross-validated the LBP coefficient based on solid phase PFAS concentration by CIC. As shown with the blue line of Fig. 3, all but one data point from the 40 μM PFOA spiked Transil^{XL} tested by CIC fall inside the 95% confidence interval (CI) of LC-MS/MS regression model. For PFOA, the resulted LBP based upon CIC was $10^{2.8\pm0.3}$ L kg^{-1}, which was comparable with the LC-MS/MS result of $10^{3.0\pm0.2}$ L kg^{-1}. At our selected initial PFOA concentration of 40 μM, the consistency between target liquid-phase LC-MS/MS and CIC-based solid/liquid-phase LBP data suggests both analytical approaches are likely suitable to obtain LBP values. The benefit of CIC analysis of lipid bilayer beads lies in its ability to quantify non-target PFAS (*i.e.*, UIOF).

The F^- had very low affinity with lipid bilayers. In this study, LBP measured by 600 μM F^- as NaF resulted in an LBP <10^1 L kg^{-1}. F^- did not enter membrane beads without the facilitation of ion carrier, thereby indicating F^- did not partition onto the Transil^{XL} lipid bilayer.[54] LBP of F^- was lower than LBP of short chain by-products, which was in turn lower than LBP of long chain parent PFOA, indicating that increasing defluorination was associated with decreased LBP. The removal of fluorine atoms from the molecular structure of PFAS accompanied by a chain shortening effect leads to a diminished affinity to lipid bilayers.[29,55] Therefore, the presence of F^- in solution with by-products of PFOA electrocatalysis was unlikely to cause artifacts or influence LBP calculation.

3.4 Applying LBP on by-products of PFOA electrocatalysis

Using LBP as an indicator of bioaccumulation potential showed a statistically significant decrease ($p < 0.05$) after 3 hours of treatment. Changes of fluorine partition on lipid bilayers and liquid of electrocatalysis samples are shown in Fig. S6.† Fig. 4A shows that LBP decreased by 31% from 850 ± 130 L kg^{-1} to 580 ± 110 L kg^{-1} in the first hour of electrocatalysis. After 3 hours of electrocatalysis, there LBP reduced by 84% to 140 ± 50 L kg^{-1}. The final LBP of electrocatalysis was between the LBP of PFHxA and PFBA, indicating UIOF existed with LBP higher than that of PFBA.

Fig. 4B shows the percent LBP remaining along with the other three analytical endpoints. A calculated residual of organofluorine, TF minus F^- was obtained, which equals UIOF + $\sum_i n_i C_i$ or AOF + NAOF, according to eqn (2) and (3). The normalized ratio of TF-F^- was significantly higher ($p < 0.05$) than the PFOA remaining at all sampling times after 1 hour, which indicated that by-products still contain organofluorine that could be captured by AOF and contribute to LBP.[56] All AOF data points after 0.5 hours and all LBP data points after 1 hour fell between PFOA degradation and TF-F^- curve, indicating effective partition of PFOA transformation products onto lipids bilayers. Even at 99% of PFOA degradation, the organofluorine residuals could still attach onto Transil^{XL} beads. Previous

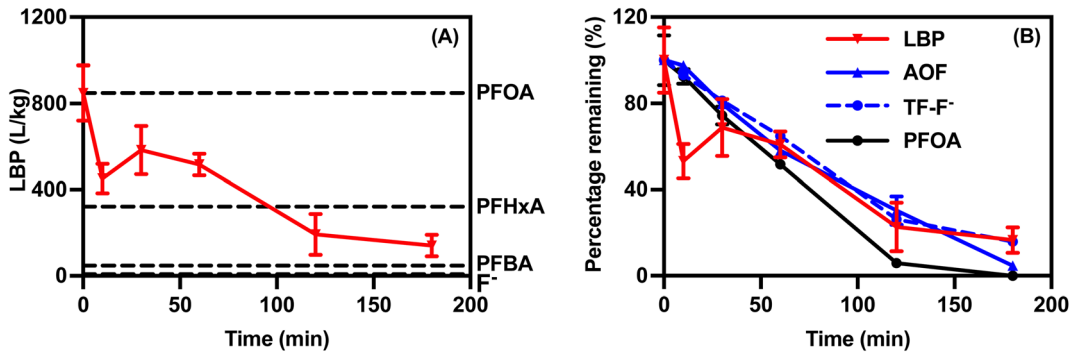

Fig. 4 Change of LBP over time. (A) Absolute LBP during electrocatalysis. LBP of target PFOA, PFHxA, PFBA and F^- are shown in dashed lines. (B) The percentage remaining of PFOA, TF-F^-, AOF, and LBP. Error bars depict standard deviations of duplicated experiments.

research utilizing *Aliivibrio fischeri* bioluminescence assay to study how PFAS treatment process impact the toxic potency concluded that UIOF degradation may cause higher decrease in bioassay activity than in target PFAS concentration.[49] However, in our case, the contribution of UIOF was too small to exhibit greater impact than target PFAS. From the discussed comparison, LBP and AOF could fill in the knowledge gap of the properties and fate of PFOA by-products the degradation and defluorination endpoints.

3.5 Relationship between target analysis and surrogate measurements

Fig. 5 shows the concentrations of PFOA, F^-, AOF, and LBP exhibited linear trends. Pearson correlation coefficients (r) of the four parameters with each other are summarized in Table S10.† F^- had negative correlation coefficients with the other three parameters. The strongest correlation happened between PFOA and F^- because F^- was the primary direct product of PFOA degradation. AOF also reveals strong correlation with PFOA and F^-, with p values for both correlations <0.001, and $r = 0.99$. The positive correlation between LBP and AOF indicates organofluorine that adsorb more strongly onto activated carbon in AOF pre-concentration are more prone to partition onto lipid bilayers. As such, AOF could be a possible indicator of bioaccumulation potential. The negative correlation between LBP and F^- implies higher mineralization correlated with likelihood to reduce bioaccumulation potential.

3.6 Comparison of treatment performance endpoint metrics

Applying the proper analysis tool was argued to be crucial in organofluorine studies, and there was a trade-off between

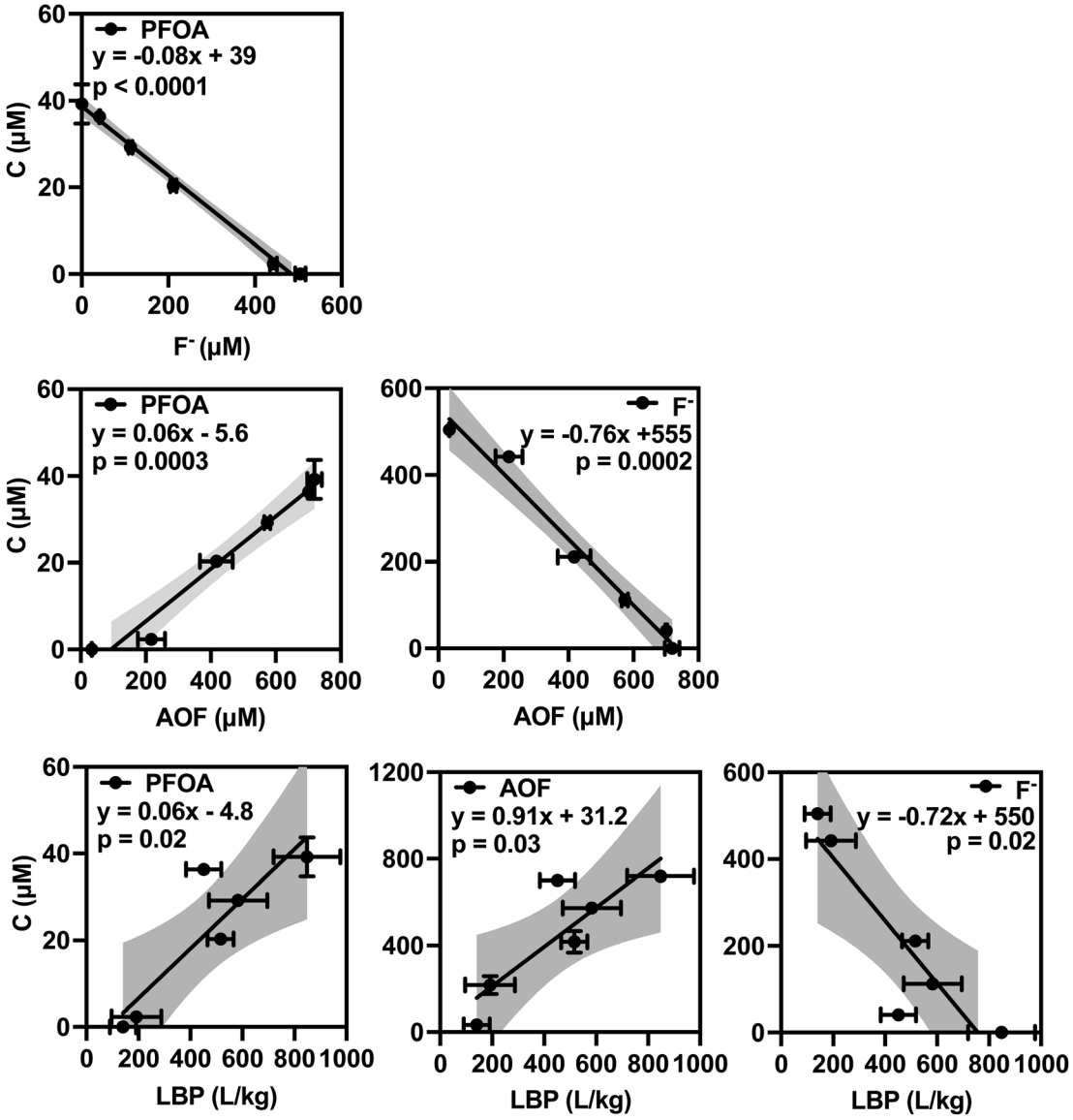

Fig. 5 Correlations between target analysis for PFOA degradation, defluorination, AOF, and LBP. Linear regression formula and significance value are given on each subplot. Shaded areas indicate the 95% confidence interval of linear regression.

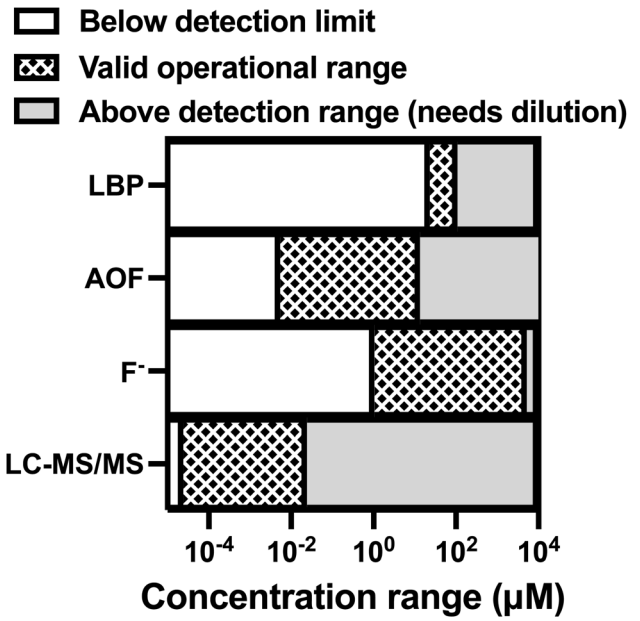

Fig. 6 Detection limits and ranges of LC-MS/MS, F^-, AOF, and LBP. Note that LC-MS/MS and LBP were measured as target PFAS compound (*i.e.*, PFOA in this study); F^- and AOF were measured as fluorine.

selectivity and inclusitivity.[57] Fig. 6 shows the analytical ranges of the endpoint metrics applied in this study, illustrating the trade-offs that PFAS treatment designers and operators will face. The LC-MS/MS target analysis has remarkably low LoQ and an uncertainty level below 10%, providing the most sensitive analysis. However, target analysis using LC-MS/MS of common PFAS represented less than 30% of the organofluorine during electrolysis. LC-MS/MS detection range spans >3 magnitudes for PFOA.

The F^- and AOF are both IC based quantification methods. F^- measured by IC has the broadest detection range (1.0 μM to 5000 μM). In this study, LoQ of AOF was limited by the maximum sample loading volume (100 mL) the autosampler syringe could hold, which in turn limited the CIC detection limit to 0.06 nmol as fluorine. The benefit of AOF was the inclusion of non-target organofluorine compounds based on their hydrophobicity.

The LBP validated by single compounds appeared viable to analyze mixtures of PFAS. However, LBP had the highest LoQ and narrowest quantification range (23–110 μM). This limitation arises from the CIC fluorine detection limit and because the Transil^{XL} kit uses a sample volume that was ~500–1000× smaller than the water volume loaded onto the AC prior to AOF quantification. The highest concentration to be applied to measure LBP was determined by the critical micelle concentration of 110 μM for PFOA.[58] As discussed in relation to Fig. 4 and 5, LBP also had larger standard errors than other analytical techniques. Consequently, LBP was probably not applicable for monitoring most industrial wastewater treatment systems where PFAS concentration ranges from ~1–10 μg L^{-1}, corresponding to <10 μg L^{-1} fluorine. However, because AOF and LBP were well correlated (Fig. 5), there is potential to use AOF as a surrogate of LBP.

4. Summary and conclusions

Electrocatalysis can break the carbon–fluorine bonds in PFAS, transforming them into lower molecular weight products with less bioaccumulation potential. Electrocatalysis with BDD anodes and cathodes effectively degraded PFOA over time, forming both target and non-target by-products. In our experimental system, the changes in PFOA were monitored over 3 hours and > 99% removal was observed. While 84% of the initial PFOA on was recovered as F^- after 3 hours, longer reaction times, greater electrode surface area, and higher energy inputs were required to reach higher levels of defluorination.

The hazard index proposed by USEPA offers a framework to assess the reduction in toxicity of treated PFAS wastewater. However, it accounts for only four target PFAS (GenX, PFBS, PFHxS, and PFNA), none of which occurred in our PFOA degradation experiments because they are not degradation by-products of PFOA. While we did detect low concentrations of PFHxA and PFBA, these PFAS are not part of the USEPA hazard index calculation. Consequently, the hazard index would be 0 despite target PFAS being detected.

Surrogate indices were explored during electrocatalysis and correlated well with the target analysis. AOF was reduced by 70% after 2 hours and 95% after 3 hours of electrocatalysis. After validating that CIC measurements of fluorine on the Transil^{XL} beads were an acceptable approach to determine LBP coefficients, LBP was applied on experimental samples collected during electrocatalysis and found an 83% reduction in LBP after treatment. A positive correlation was observed between LBP and AOF. Transformation by-products with lower AOF recovery were likely to be less bioaccumulative.

Considering the advantage of low detection limit, and the ease to operate, using AOF as a surrogate measure, not for toxicity *per se* but for assessing bioaccumulation potential, emerged as an intriguing conceptual and quantifiable approach to monitor electrocatalytic treatment.

Author contributions

ZL-investigation, writing original draft, formal analysis, conceptualization, data curation, validation, visualization, writing-review and editing; ME-conceptualization, supervision, validation, formal analysis, writing-review and editing; SGS-conceptualization, methodology, resources, funding acquisition, project administration, writing-review and editing; FP-conceptualization, methodology, writing-review and editing; PW-corresponding, conceptualization, resources, data curation, formal analysis, writing original draft, writing-review and editing, funding acquisition, project administration, supervision.

Conflicts of interest

There are no conflicts to declare.

Acknowledgements

This project was funded by Semiconductor Research Corporation GRC Task 2818.005. We acknowledge SRC committee for funding this project. Laurel Passantino provided technical editing. Metals Environmental and Terrestrial Analytical Laboratory provided surface characterization data of activated carbon.

References

1 E. Tavasoli, J. L. Luek, J. P. Malley, Jr. and P. J. Mouser, *Environ. Sci.: Processes Impacts*, 2021, **23**, 903–913.
2 J. Yao, Y. Pan, N. Sheng, Z. Su, Y. Guo, J. Wang and J. Dai, *Environ. Sci. Technol.*, 2020, **54**, 13389–13398.
3 F. Dong, Y. Pan, J. Zhang, J. Hu, Y. Luo, J. Tang, J. Dai and N. Sheng, *Environ. Sci. Technol.*, 2023, **57**(48), 19442–19452.
4 P. Jacob, K. A. Barzen-Hanson and D. E. Helbling, *Environ. Sci. Technol.*, 2021, **55**, 2346–2356.
5 P. Jacob and D. E. Helbling, *Environ. Sci. Technol.*, 2023, **57**, 12819–12828.
6 X. C. Hu, D. Q. Andrews, A. B. Lindstrom, T. A. Bruton, L. A. Schaider, P. Grandjean, R. Lohmann, C. C. Carignan, A. Blum, S. A. Balan, C. P. Higgins and E. M. Sunderland, *Environ. Sci. Technol. Lett.*, 2016, **3**, 344–350.
7 J. Campo, M. Lorenzo, F. Perez, Y. Pico, M. Farre and D. Barcelo, *Environ. Res.*, 2016, **147**, 503–512.
8 D. Mussabek, L. Ahrens, K. M. Persson and R. Berndtsson, *Chemosphere*, 2019, **227**, 624–629.
9 M. W. Sima and P. R. Jaffe, *Sci. Total Environ.*, 2021, **757**, 143793.
10 J. Zhang, L. Gao, D. Bergmann, T. Bulatovic, A. Surapaneni and S. Gray, *Sci. Total Environ.*, 2023, **854**, 158796.
11 L. Teunen, L. Bervoets, C. Belpaire, M. De Jonge and T. Groffen, *Environ. Sci. Eur.*, 2021, **33**, 39.
12 N. Macorps, K. Le Menach, P. Pardon, S. Guerin-Rechdaoui, V. Rocher, H. Budzinski and P. Labadie, *Environ. Pollut.*, 2022, **303**, 119165.
13 P. Pierozan, D. Cattani and O. Karlsson, *Sci. Total Environ.*, 2022, **808**, 151945.
14 B. P. Rickard, I. Rizvi and S. E. Fenton, *Toxicology*, 2022, **465**, 153031.
15 V. Ehrlich, W. Bil, R. Vandebriel, B. Granum, M. Luijten, B. Lindeman, P. Grandjean, A. M. Kaiser, I. Hauzenberger, C. Hartmann, C. Gundacker and M. Uhl, *Environ. Health*, 2023, **22**, 19.
16 USEPA, *PFAS National Primary Drinking Water Regulation*, **https://www.epa.gov/system/files/documents/2024-04/pfas-npdwr_fact-sheet_general_4.9.24v1.pdf**.
17 H. S. G., *PFAS in Biosolids: A Review of State Efforts & Opportunities for Action*, 2023.
18 NACWA, *Biosolids and PFAS: Maintaining Management Options is Critical to Communities and Sustainability*, 2022.
19 J. Kidd, E. Fabricatore and D. Jackson, *Sci. Total Environ.*, 2022, **836**, 155523.
20 M. DeNicola, Z. Lin, O. Quiñones, B. Vanderford, M. Song, P. Westerhoff, E. Dickenson and D. Hanigan, *Sci. Total Environ.*, 2023, **905**, 166971.
21 A. L. B. Forster, Y. Zhang, D. C. Westerman and S. D. Richardson, *Water Res.*, 2023, **235**, 119859.
22 K. Zhang, S. Wiseman, J. P. Giesy and J. W. Martin, *Environ. Sci. Technol.*, 2016, **50**, 6574–6582.
23 L. Zhao, Y. Zhang, L. Zhu, X. Ma, Y. Wang, H. Sun and Y. Luo, *Environ. Sci. Technol. Lett.*, 2017, **4**, 391–398.
24 E. I. Loi, L. W. Yeung, S. Taniyasu, P. K. Lam, K. Kannan and N. Yamashita, *Environ. Sci. Technol.*, 2011, **45**, 5506–5513.
25 R. Gronnestad, B. P. Vazquez, A. Arukwe, V. L. B. Jaspers, B. M. Jenssen, M. Karimi, J. L. Lyche and A. Krokje, *Environ. Sci. Technol.*, 2019, **53**, 13390–13397.
26 F. Chen, Z. Gong and B. C. Kelly, *Sci. Total Environ.*, 2016, **568**, 33–41.
27 F. Menger, J. Pohl, L. Ahrens, G. Carlsson and S. Orn, *Chemosphere*, 2020, **245**, 125573.
28 L. B. Barber, H. M. Pickard, D. A. Alvarez, J. Becanova, S. H. Keefe, D. R. LeBlanc, R. Lohmann, J. A. Steevens and A. M. Vajda, *Environ. Sci. Technol.*, 2023, **57**, 5544–5557.
29 S. T. J. Droge, *Environ. Sci. Technol.*, 2019, **53**, 760–770.
30 R. K. Singh, N. Multari, C. Nau-Hix, S. Woodard, M. Nickelsen, S. Mededovic Thagard and T. M. Holsen, *Environ. Sci. Technol.*, 2020, **54**, 13973–13980.
31 A. B. Nienhauser, M. S. Ersan, Z. Lin, F. Perreault, P. Westerhoff and S. Garcia-Segura, *J. Environ. Chem. Eng.*, 2022, **10**(2), 107192.
32 Z. Chen, X. Wang, H. Feng, S. Chen, J. Niu, G. Di, D. Kujawski and J. C. Crittenden, *Environ. Sci. Technol.*, 2022, **56**, 14409–14417.
33 L. Duan, B. Wang, K. Heck, S. Guo, C. A. Clark, J. Arredondo, M. Wang, T. P. Senftle, P. Westerhoff, X. Wen, Y. Song and M. S. Wong, *Environ. Sci. Technol. Lett.*, 2020, **7**, 613–619.
34 J. Cui, P. Gao and Y. Deng, *Environ. Sci. Technol.*, 2020, **54**, 3752–3766.
35 E. W. Tow, M. S. Ersan, S. Kum, T. Lee, T. F. Speth, C. Owen, C. Bellona, M. N. Nadagouda, A. M. Mikelonis, P. Westerhoff, C. Mysore, V. S. Frenkel, V. deSilva, W. S. Walker, A. K. Safulko and D. A. Ladner, *AWWA Water Sci.*, 2021, **3**, 1–23.
36 S. P. Lenka, M. Kah and L. P. Padhye, *Water Res.*, 2021, **199**, 117187.
37 B. I. Escher and K. Fenner, *Environ. Sci. Technol.*, 2011, **45**, 3835–3847.
38 G. Ersan, M. S. Ersan, F. Perreault and S. Garcia-Segura, *J. Environ. Chem. Eng.*, 2023, **11**(6), 111369.
39 Y. Miyake, N. Yamashita, P. Rostkowski, M. K. So, S. Taniyasu, P. K. Lam and K. Kannan, *J. Chromatogr. A*, 2007, **1143**, 98–104.
40 M. S. Ersan, B. Wang, M. S. Wong and P. Westerhoff, *Chemosphere*, 2023, **349**, 140865.
41 Y. Han, V. F. Pulikkal and M. Sun, *ACS ES&T Water*, 2021, **1**, 1474–1482.
42 R. Aro, U. Eriksson, A. Karrman, I. Reber and L. W. Y. Yeung, *iScience*, 2021, **24**, 102968.

43 W. C. Hou, B. Y. Moghadam, C. Corredor, P. Westerhoff and J. D. Posner, *Environ. Sci. Technol.*, 2012, **46**, 1869–1876.
44 S. Sukeesan, N. Boontanon and S. K. Boontanon, *Environ. Technol. Innovation*, 2021, **23**, 101655.
45 N. B. Uner, P. Baldaguez Medina, J. L. Dinari, X. Su and R. M. Sankaran, *Langmuir*, 2022, **38**, 8975–8986.
46 J. Radjenovic, N. Duinslaeger, S. S. Avval and B. P. Chaplin, *Environ. Sci. Technol.*, 2020, **54**, 14815–14829.
47 S. J. Smith, M. Lauria, C. P. Higgins, K. D. Pennell, J. Blotevogel and H. P. H. Arp, *Environ. Sci. Technol.*, 2024, **58**(6), 2587–2590.
48 Y. Pan and D. E. Helbling, *Water Res.*, 2023, **244**, 120497.
49 S. J. Smith, M. Lauria, L. Ahrens, P. McCleaf, P. Hollman, S. Bjalkefur Seroka, T. Hamers, H. P. H. Arp and K. Wiberg, *ACS ES&T Water*, 2023, **3**, 1201–1211.
50 V. H. Adams, M. J. McAtee and M. S. Johnson, *Integr. Environ. Assess. Manage.*, 2017, **13**, 852–860.
51 S. Taniyasu, K. Kannan, L. W. Yeung, K. Y. Kwok, P. K. Lam and N. Yamashita, *Anal. Chim. Acta*, 2008, **619**, 221–230.
52 C. E. Schaefer, C. Higgins, T. Strathmann and I. Ferguson, *Investigating Electrocatalytic and Catalytic Approaches for in Situ Treatment of Perfluoroalkyl Contaminants in Groundwater (ER-2424)*, 2020.
53 A. Loidl-Stahlhofen, T. Hartmann, M. Schöttner, C. Röhring, H. Brodowsky, J. Schmitt and J. Keldenich, *Pharm. Res.*, 2001, **18**, 1782–1788.
54 C. Gonzalo and J. A. Camargo, *Ecol. Indic.*, 2012, **20**, 244–251.
55 N. J. M. Fitzgerald, A. Wargenau, C. Sorenson, J. Pedersen, N. Tufenkji, P. J. Novak and M. F. Simcik, *Environ. Sci. Technol.*, 2018, **52**, 10433–10440.
56 M. Mirabediny, J. Sun, T. T. Yu, B. Akermark, B. Das and N. Kumar, *Chemosphere*, 2023, **321**, 138109.
57 C. A. McDonough, J. L. Guelfo and C. P. Higgins, *Curr Opin Environ Sci Health*, 2019, **7**, 13–18.
58 S. Yang, F. Xu, F. Wu, S. Wang and B. Zheng, *Sci. Total Environ.*, 2014, **470–471**, 677–683.